J. Electrochem. Sci. Eng. **16** (2026) 3133; https://doi.org/10.5599/jese.3133

Open Access : : ISSN 1847-9286
https://pub.iapchem.org/ojs/index.php/JESE

Original scientific paper

Ultrasound-assisted alkaline water electrolysis in a membrane-separated H-type cell: a device-scale benchmark under galvanostatic operation

Zeng ChenHongWen[1], Yew Heng Teoh[1,✉], Heoy Geok How[2], Mohamad Yusof Idroas[1] and Thanh Danh Le[3]

[1]*School of Mechanical Engineering, Tuanku Syed Sirajuddin Engineering Campus, Universiti Sains Malaysia, 14300 Nibong Tebal, Pulau Pinang, Malaysia*
[2]*Department of Engineering, UOW Malaysia KDU Penang University College, Batu Kawan Campus, PMT755, Persiaran Cassia Barat 3, Bandar Cassia, 14110, Simpang Ampat, Malaysia*
[3]*College of Technology and Design, University of Economics Ho Chi Minh City (UEH), 59C Nguyen Dinh Chieu Street, Xuan Hoa Ward, Ho Chi Minh City 700000, Viet Nam*

Corresponding Authors: ✉*yewhengteoh@usm.my*; Tel.: +604-5996325; Fax: +604-5941025

Received: November 24, 2025; Accepted: April 27, 2026; Published: May 12, 2026

Abstract

Reported benefits of ultrasound in alkaline water electrolysis remain difficult to compare because apparent gains can be influenced by thermal drift, inconsistent energy-accounting boundaries, and differences in reactor geometry. Here, we provide a conservative benchmark of ultrasound-assisted alkaline water electrolysis in a small, membrane-separated H-type cell operated galvanostatically in 2.0 M NaOH at 0.6, 0.8, and 1.0 A. Silent electrolysis, low-amplitude ultrasound, and high-amplitude ultrasound were compared over a unified 300 s window while maintaining the catholyte near the hydrogen-evolving electrode at 32-34 °C. Under these tightly controlled conditions, ultrasound produced small but consistent device-internal effects: collected H_2 output increased by about 1 %, purity-corrected Faradaic efficiency remained essentially unchanged at around 66 %, and the average cell voltage decreased by approximately 0.09 to 0.29 V, corresponding to a 1.6 to 2.1 % reduction in specific electrical energy consumption on an electrolyzer-electrical basis. These results are most consistent with relief of bubble-related and near-electrode transport losses, rather than the emergence of a new reaction pathway or a large change in intrinsic reaction kinetics. At 1.0 A, varying ultrasonic amplitude further indicated a practical operating window in which moderate ultrasound minimized electrolyzer-electrical SEC, whereas higher amplitude maximized instantaneous hydrogen throughput but caused visible graphite-anode degradation in the present geometry. The present results, therefore, do not establish a full-system energy benefit; instead, they provide a conservative, device-internal benchmark for assessing

when, and to what extent, ultrasound may remain useful under rigorously controlled conditions. Future studies should extend this framework to reduced-gap cells, advanced electrodes, and full system-level accounting that explicitly includes acoustic power and balance-of-plant loads.

Keywords
Electrochemical water splitting; sono-electrolysis; device-scale benchmark; hydrogen production

Introduction

Low-carbon hydrogen is widely regarded as an essential pillar in net-zero strategies for hard-to-abate sectors such as chemicals, steel and heavy transport, with global roadmaps assigning a central role to water electrolysis powered by renewable electricity [1-3]. Among the available technologies, alkaline water electrolysis (AWE) remains the most mature and widely deployed option due to its relatively low capital cost and the use of abundant, non-noble catalysts [1,2,4]. Nevertheless, the overall energy efficiency of AWE is still constrained by a combination of activation losses at the hydrogen and oxygen evolution reactions, ohmic drops across the diaphragm or membrane and electrolyte, and mass-transport limitations linked to gas bubble evolution at the electrodes [4-6]. Recent analyses underscore that gas bubbles can dominate local transport resistances and effective current distribution in both proton exchange membrane (PEM) and alkaline electrolyzers, making bubble management a key lever for improving performance [5-7]. At the same time, large-scale deployment requires AWE systems that can deliver stable operation and predictable efficiency under realistic, dynamically varying loads, which in turn calls for robust, experimentally grounded benchmarks of process-intensification strategies [1,2,4].

Power ultrasound has emerged as a promising process-intensification tool across a wide range of electrochemical and sonochemical applications [8-12]. In electrochemical systems, acoustic cavitation, microstreaming and pressure oscillations can enhance mass transfer, promote bubble detachment and modify near-electrode hydrodynamics, thereby influencing both reaction rates and energy consumption [12-14]. Recent studies on ultrasound-assisted hydrogen production and water electrolysis show that ultrasonication can alter hydrogen bubble size, growth and detachment behaviour [7,15-17] reduce bubble-induced resistances and, in some cases, lower cell voltage or specific energy consumption at fixed current [13,18]. Reviews on ultrasound-assisted electrochemical processes and ultrasonic reactor design further highlight the importance of reactor geometry, acoustic frequency and intensity in determining the balance between beneficial bubble management and detrimental heating or erosion [9-11]. In the specific context of sono-electrolysis, coupled numerical-experimental work has demonstrated the feasibility of membraneless ultrasonic reactors powered by photovoltaics [18,19], while broader surveys emphasise both the potential of ultrasound to support “green hydrogen” and the current lack of systematic benchmarks in realistic alkaline configurations [13,14]. In parallel, significant progress has been made on materials-driven improvements in AWE, such as advanced electrocatalysts, tailored diaphragms and anion-exchange membranes, including recent contributions that focus on electrocatalyst design and electrochemical behaviour toward water electrolysis. However, there is still limited experimental evidence that quantifies, in a controlled and comparable manner, what ultrasound can and cannot achieve in simple, membrane-separated alkaline cells where all electrical and gas-analysis corrections are explicitly accounted for.

Against this background, the present work uses a compact, membrane-separated H-type alkaline electrolyzer to establish a conservative, device-scale benchmark for ultrasound-assisted water electrolysis under tightly controlled galvanostatic conditions. Building on recent metrology- and boundary-aware assessments of sono-electrolysis, including our own review [20], which emphasized explicit SEC boundaries, controlled thermal conditions, and window-based interpretation of ultrasound effects, the aim here is not to claim a generalized or system-level efficiency gain, but to determine whether any reproducible device-internal benefit remains once temperature, gas metrology, and performance boundaries are explicitly controlled. In 2.0 M NaOH, we therefore compare silent electrolysis with low- and high-amplitude ultrasound at 0.6, 0.8, and 1.0 A, while quantifying hydrogen production rate, purity-corrected Faradaic efficiency, time-averaged cell voltage, and specific energy consumption on an electrolyzer-electrical basis. Rather than pursuing record performance, this study is designed to clarify the practical magnitude and origin of any ultrasound effect in a simple alkaline configuration relevant to bubble management, and to identify a realistic operating window together with its limitations. In this sense, the present H-type cell is intended as a lower-bound benchmark: a controlled reference for judging when ultrasound provides a genuine bubble- and transport-related benefit, and when further gains must instead come from improved cell architecture, electrode design, and full system-level energy accounting that explicitly includes acoustic power and auxiliary loads.

Experimental

This study used a membrane-separated H-type electrolyzer operated at constant current under two regimes: electrolysis (Elec) and sono-electrolysis (Sono). All runs followed a unified protocol to ensure reproducibility and to isolate the effect of ultrasound under matched electrochemical conditions. The experimental setup is shown in Figure 1 (photograph) and Figure 2 (schematic of H-type cell-bath coupling).

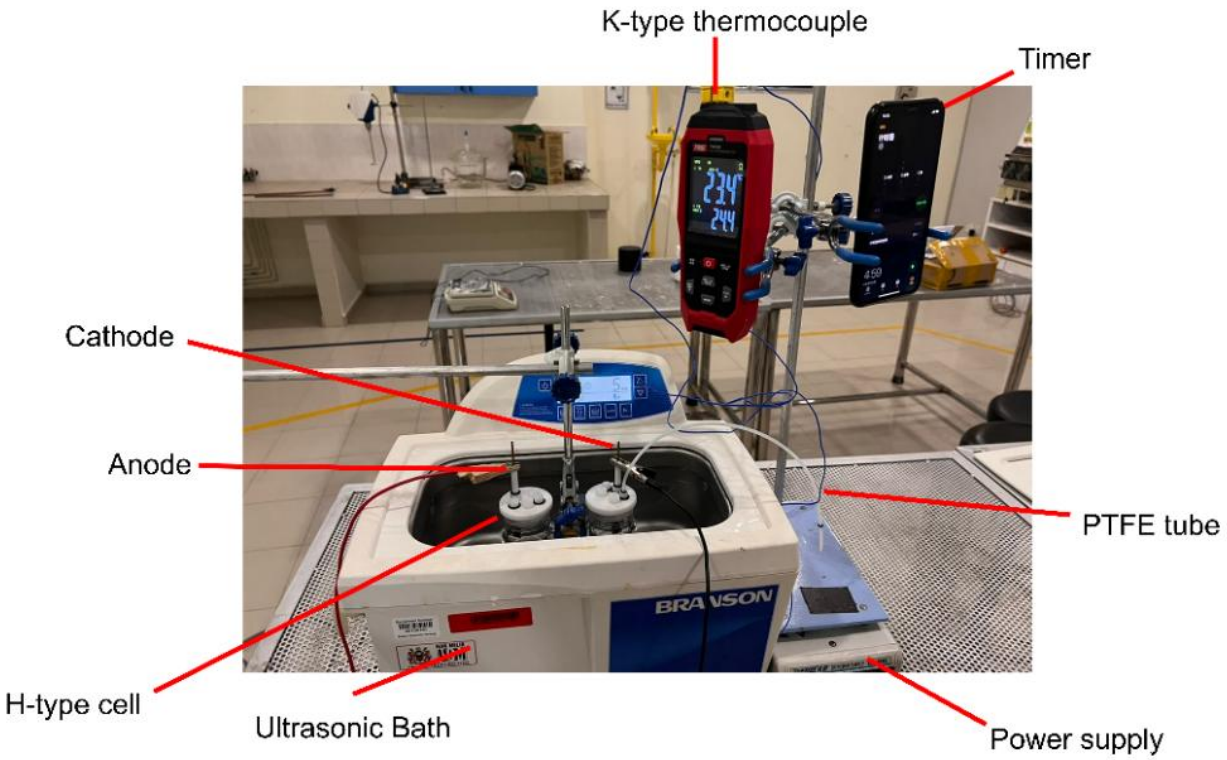

***Figure 1**. Photograph of the experimental setup*

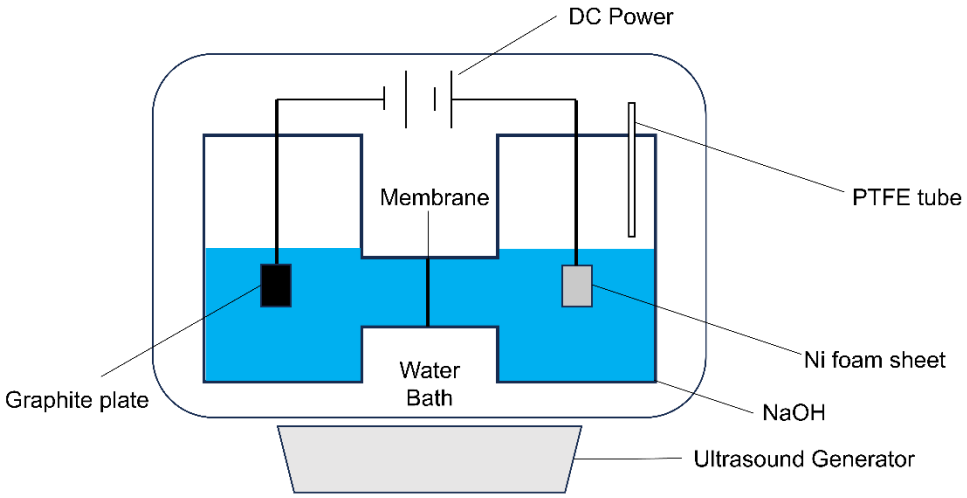

***Figure 2**. Experimental setup (schematic)*

Apparatus and materials

A two-chamber borosilicate H-type cell (50 mL per chamber) was separated by a Nafion N117 membrane (ϕ = 30 mm). Each chamber was filled with 35 mL of freshly prepared 2 M NaOH. The anode was a graphite plate and the cathode a nickel-foam sheet; both had a 1 cm² immersed geometric area, were mounted vertically at fixed depth, and were placed symmetrically about the membrane.

The cell was partially immersed (≈ 2/3 height) in a Bransonic CPX3800H-E ultrasonic bath (40 kHz; manufacturer-rated acoustic power 110 W; two settings used: 70 and 100 %; nominal intensities 0.177/0.253 W cm^{-2}). RXN-305D direct-current (DC) source supplied constant current (0.6, 0.8 and 1.0 A). Local catholyte temperature was measured with a K-type thermocouple positioned 3 to 5 mm from the cathode surface. Hydrogen was collected by inverted water displacement via a short polytetrafluoroethylene (PTFE) tube; gas temperature was monitored near the outlet. Gas purity was periodically measured by gas chromatography (GC) and used as a correction factor in Faradaic-efficiency calculations.

Graphite anodes were mechanically polished, ultrasonically cleaned, acid-washed in 0.1 M HCl for 10 min, and rinsed with distilled water. Ni-foam cathodes were dipped in 0.5 M HCl for 5 min and rinsed thoroughly. Nafion N117 was soaked in distilled water for 24 h prior to use. Fresh electrodes and electrolyte were used in every run. Key specifications are summarized in Table 1 (ultrasonic bath) and Table 2 (H-type cell).

***Table 1.** Ultrasonic bath (Bransonic CPX3800H-E) specifications*

Component	Specification
Frequency, kHz	40
Rated ultrasonic power, W	110
Acoustic power intensity, W cm^{-2}	0.177/0.253
Tank capacity, L	5.7
Overall dimensions (L×W×H), mm	397×317×377
Tank dimensions (L×W×H), mm	290×150×150
Heating	Adjustable to a maximum of 69 °C
Control panel	Mechanical push-button control panel
Drain	Drain outlet on the sidewall
Material	Body constructed of chemical-resistant plastic

Table 2. *H-type electrolysis cell specifications*

Component	Specification
Cell type	Two-chamber H-type electrolyzer
Chamber volume, mL	50, each
Inter chamber diameter, mm	40
Chamber height (internal), mm	45
Inter-chamber connector	Central bridge port
Membrane diameter, mm	30 (circular)
Membrane type	Nafion N117 proton-exchange membrane
Electrode ports	3 ports, ϕ6.2 mm each lid
Gas ports	2 ports, ϕ3.1 mm each lid
Inter-chamber passage diameter, mm	9 mm
Lid material	PTFE (polytetrafluoroethylene)
Chamber material	Borosilicate glass
Sealing method	Screw-locking with PTFE compression gaskets
Tubing	PTFE outlet tubing

Operating procedure

For each trial, 35 mL of 2 M NaOH was loaded into each chamber; the electrodes (1 cm²) were set to identical immersion depths. The assembled H-type cell was lowered into the ultrasonic bath until the electrolyte column was submerged while keeping the headspace dry. The bath was pre-run for ≈ 2 min to stabilize acoustic output and liquid temperature. Electrolysis was then conducted at constant current (0.6/0.8/1.0 A) for 300 s. Catholyte temperature (near-electrode, 3 to 5 mm) was controlled by an external water-bath buffering, which limited heating to ≈ 32 to 34 °C (ΔT ≈ 2 °C) and avoided thermal bias. Gas was collected by displacement into a calibrated cylinder; gas temperature was recorded near the outlet. Sono runs followed the identical sequence with ultrasound ON throughout. Each condition was repeated n = 3.

Table 3 lists the operating parameters (electrolyte, current, duration, ultrasound setting, hydrogen-purity baseline determined by gas chromatography, mean cell-voltage logging and electrode areas). No post-smoothing or statistical filtering was applied.

Table 3*. Experimental operating parameters*

Parameter	Setting
Electrolyte	2 M NaOH, 35 mL per chamber
Current, A	0.6/0.8/1.0 (constant)
Duration, s	300
Ultrasound	OFF/ON
H_2 purity, %	65
Mean cell voltage	Logged each run
Cathode surface area, cm²	1
Anode surface area, cm²	1

Data reduction and performance analysis

Unless stated otherwise, all symbols follow SI units and are defined at first use below. Gas-based quantities are evaluated over the 0 to 300 s accumulation window (triplicate, reported as mean ± standard deviation (SD)), while electrical energy is evaluated using a steady-window voltage estimate defined in this section. No smoothing or outlier removal is applied; the reported uncertainty reflects run-to-run reproducibility.

To convert the wet displaced volume to dry moles of hydrogen, the water-vapor correction to the ideal-gas relation is applied as in Equation (1):

$$n_{\mathrm{H_2}} = \frac{\left(P - P_{\mathrm{H_2O}}\right)V}{RT_{\mathrm{g}}} \tag{1}$$

where $n_{\mathrm{H_2}}$ / mol is the amount of hydrogen, P = 100.7 kPa is the ambient pressure, $P_{\mathrm{H_2O}}$ is the saturated vapor pressure at the measured outlet-gas temperature T_{g}, V is the measured wet gas volume and R = 8.314 J mol$_{-1}$ K^{-1} is the ideal-gas constant.

As given in Equation (2), a gas chromatography-based hydrogen-purity correction factor (f_{p}) is applied as a direct proportional correction to account for residual moisture and dissolved-gas effects:

$$n_{\mathrm{H_2,corr}} = n_{\mathrm{H_2}} f_{\mathrm{p}} \tag{2}$$

where $n_{\mathrm{H_2,corr}}$ is the corrected hydrogen amount and f_{p} is the hydrogen-purity correction factor obtained from the gas chromatography measurement (baseline ≈ 0.65 under the present configuration).

As shown in Equation (3), when reporting volumetric quantities on a common basis, the corrected hydrogen amount is converted to the gas volume at standard temperature and pressure (STP):

$$V_{\mathrm{H_2,STP}} = n_{\mathrm{H_2,corr}} \frac{RT_{\mathrm{STP}}}{P_{\mathrm{STP}}} \tag{3}$$

where $V_{\mathrm{H_2\,STP}}$ is the corrected hydrogen volume at STP, T_{STP} = 273.15 K, and P_{STP} = 101.325 kPa (1 atm).

Accordingly, the volumetric hydrogen production rate is given by Equation (4):

$$r_{V,\mathrm{H_2}} = \frac{V_{\mathrm{H_2,STP}}}{t} \tag{4}$$

where $r_{V,\mathrm{H_2}}$ is the volumetric hydrogen production rate and t is the run duration.

The corresponding molar hydrogen production rate is given by Equation (5):

$$r_{n,\mathrm{H_2}} = \frac{n_{\mathrm{H_2,corr}}}{t} \tag{5}$$

where $r_{n,\mathrm{H_2}}$ is the molar hydrogen production rate.

In Equations (4) and (5), t = 300 s is the run duration.

For charge-limited benchmarking, the theoretical hydrogen amount predicted by Faraday's law is given by Equation (6):

$$n_{\mathrm{th}} = \frac{It}{2\mathrm{F}} \tag{6}$$

where n_{th} is the theoretical hydrogen amount, I is the applied current, t = 300 s is the electrolysis duration and F = 96485 C mol^{-1} is Faraday's constant.

The Faradaic efficiency (η_{F} / %) was then calculated as the ratio between corrected experimental hydrogen amount and the theoretical value, as shown in Equation (7):

$$\eta_F = \frac{n_{\mathrm{H_2,corr}}}{n_{\mathrm{th}}} 100 \tag{7}$$

The electrical energy input over the 300 s run was evaluated in continuous form as shown in Equation (8):

$$E_{\mathrm{elec}} = \int_0^t U(t) I \, \mathrm{d}t \tag{8}$$

where E_{elec} is the electrical energy input and $U(t)$ is the instantaneous cell voltage as a function of time.

In practice, the electrical energy was evaluated using a steady-window mean voltage ($\bar{U}$) computed from uniformly spaced voltage samples within the 0-300 s window, as given in Equations (9) and (10):

$$E_{\text{elec}} \approx \bar{U} I t \tag{9}$$

$$\bar{U} = \frac{1}{N}\sum_{i=1}^{N} U(t_i) \tag{10}$$

where N is the total number of voltage samples and $U(t_i)$ is the voltage measured at sampling time t_i.

To link the gas yield with the electrical energy input, the hydrogen mass was calculated using Equation (11):

$$m_{\text{H}_2} = n_{\text{H}_2,\text{corr}} M_{\text{H}_2} \tag{11}$$

where m_{H_2} is the hydrogen mass and M_{H_2} = 2.016 g mol^{-1} is the molar mass of hydrogen.

The specific electrical energy consumption (SEC), reported here on an electrolyzer-electrical basis, was then calculated with explicit conversion from J to kWh using Equation (12):

$$\text{SEC} = \frac{E_{\text{elec}}}{3.6\times10^6\, m_{\text{H}_2}} = \frac{\bar{U} I t}{3.6\times10^6\, n_{\text{H}_2}{}^{\text{corr}} M_{\text{H}_2}} \tag{12}$$

where SEC is the specific electrical energy consumption in kWh kg^{-1} H_2.

The energy efficiency on the higher heating value (HHV) basis follows directly from Equation (13):

$$\eta_{\text{E}} = \frac{39.4}{\text{SEC}} 100 \tag{13}$$

where η_{E} / % is the HHV-based electrical energy efficiency, and HHV denotes the higher heating value of hydrogen, taken here as 39.4 kWh kg^{-1} H_2.

Finally, to relate the energetic comparison to an electrical signature under identical current, the inter-mode voltage difference and its steady-window mean were defined by Equations (14) and (15):

$$\Delta V(t) = U_{\text{Elec}}(t) - U_{\text{Sono}}(t) \tag{14}$$

$$\overline{\Delta V} = \frac{1}{N}\sum_{i=1}^{N} \Delta V(t_i) \tag{15}$$

where $\Delta V(t)$ is the instantaneous voltage difference between silent electrolysis and sono-electrolysis, $U_{\text{Elec}}(t)$ is the cell voltage in the silent mode, $U_{\text{Sono}}(t)$ is the cell voltage in the sonicated mode, and $\overline{\Delta V}$ is the time-averaged voltage difference.

This voltage-based linkage is examined in the following cell-voltage analysis.

Results and discussion

Unless otherwise stated, all quantities are reported as the mean ± standard deviation across three independent runs for each condition, evaluated over the unified 0 to 300 s measurement window. Hydrogen volumes and rates are based on water-displacement measurements corrected for ambient pressure, water vapor saturation and tubing dead volume. Purity-corrected Faradaic efficiencies (FE) were calculated from the measured hydrogen volume fraction in the collected gas, while specific energy consumption (SEC, kWh kg^{-1} H_2) and HHV-based electrical energy efficiency (EE, %) were evaluated on an electrolyzer-electrical basis using the higher heating value (HHV) of hydrogen (39.4 kWh kg^{-1} H_2). The catholyte temperature measured 3-5 mm from the cathode remained within 32 to 34 °C throughout all tests.

In the following, “electrolysis” denotes the silent mode (ultrasound OFF) and “sono-electrolysis” the mode with the ultrasonic bath operated at the nominal amplitude used in this study, unless otherwise specified. All experiments were conducted in 2.0 M NaOH at constant current (0.6, 0.8

and 1.0 A) in the same H-type cell with identical membrane, electrodes and tubing, so that performance differences can be attributed to the presence or absence of ultrasound and to changes in ultrasonic amplitude.

Hydrogen production and Faradaic efficiency

Hydrogen production

Under constant-current operation and tightly limited temperature excursions, any change in hydrogen throughput must arise from interfacial and near-electrode processes rather than from variations in charge input. As summarized in Figure 3, the collected H_2 volume over 300 s increases monotonically with current under both electrolysis and sono-electrolysis. At each fixed current, sonication yields a higher collected volume, indicating a small but consistent throughput increase under acoustic assistance. Specifically, at 1.0 A the sonicated volume exceeds the electrolysis case by 0.4 mL (≈1.0 %); at 0.8 A by 0.33 mL (≈1.03 %); and at 0.6 A by 0.1 mL (≈0.42 %). The absolute volumes underlying these contrasts are 40.33 *vs.* 39.93 mL (1.0 A), 32.40 *vs.* 32.07 mL (0.8 A), and 24.10 *vs.* 24.00 mL (0.6 A) for sono-electrolysis and electrolysis, respectively.

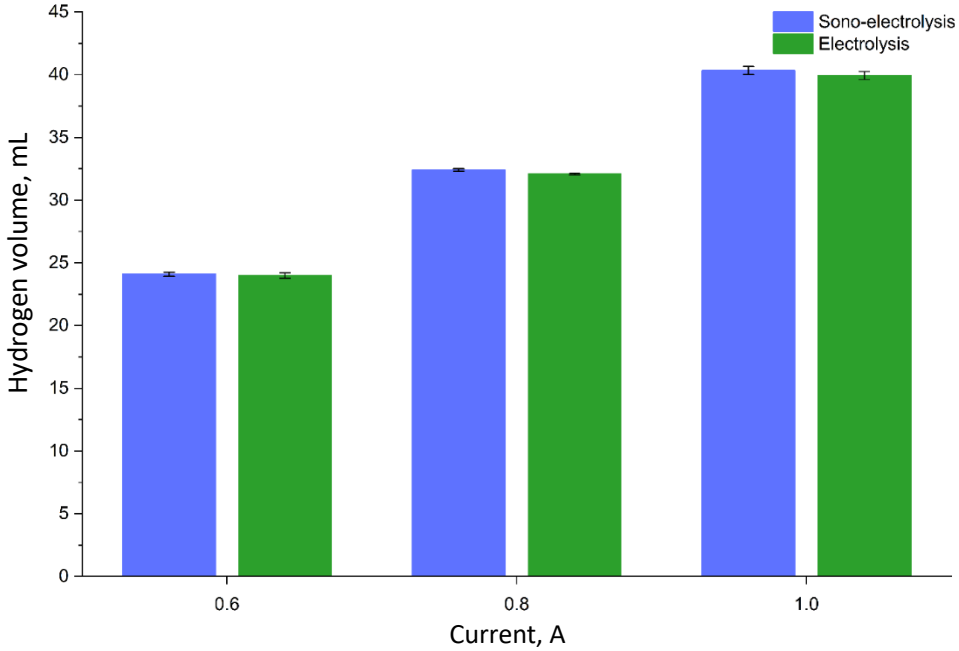

***Figure 3**. Hydrogen volume collected in 300 s at different currents*

Rate-level behaviour mirrors the volume trends. As shown in Figure 4b, the average hydrogen generation rate scales with current and remains higher under sonication at all set points. At 1.0 A, the sonicated rate exceeds the electrolysis benchmark by 0.045 mL min^{-1} (≈0.98 %), with corresponding advantages of 0.036 mL min^{-1} (≈0.97 %) at 0.8 A and 0.0282 mL min^{-1} (≈1.03 %) at 0.6 A. The underlying pairwise values are 4.64 *vs.* 4.59 mL min^{-1} (1.0 A), 3.73 *vs* 3.69 mL min^{-1} (0.8 A), and 2.77 *vs.* 2.74 mL min^{-1} (0.6 A) for sono-electrolysis and electrolysis, respectively.

Taken together, Figure 3 and Figure 4b show that ultrasound yields a modest but repeatable increase in hydrogen throughput without altering the galvanostatic current. This behaviour is consistent with cavitation-assisted bubble removal and boundary-layer renewal that expand the effective active area and mitigate transport limitations at gas-evolving interfaces. Numerical-experimental studies of ultrasonic alkaline electrolysis have shown that ultrasound can reduce the critical bubble detachment diameter, shorten residence times and decrease bubble surface coverage, thereby supporting slightly higher gas-evolution rates at fixed current [21,22]. Reviews of

sono-electrochemistry similarly report small but reproducible rate enhancements at constant current, primarily attributed to improved gas removal and near-electrode mixing rather than to changes in hydrogen evolution reaction (HER) / oxygen evolution reaction (OER) pathways [4,21,22].

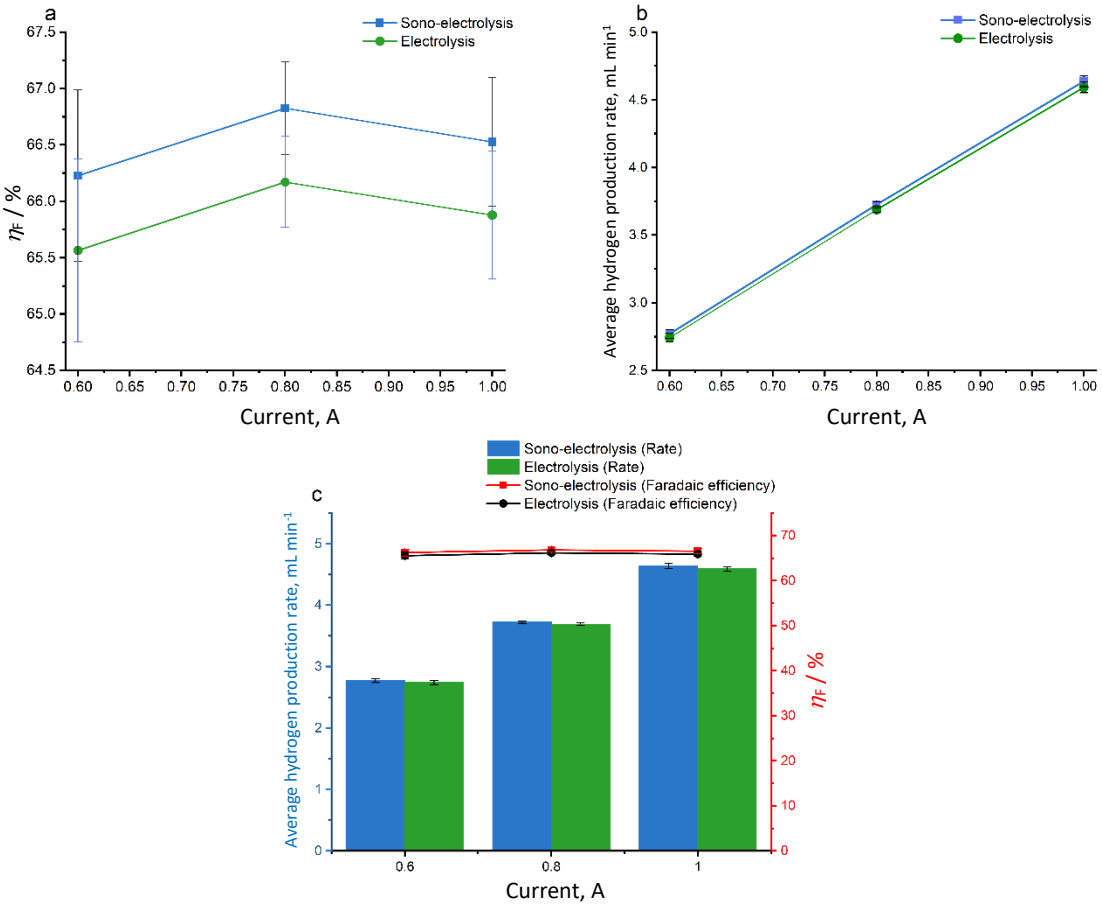

Figure 4. *(a) FE* vs. *current; (b) average H_2 generation rate* vs. *current; (c) bar chart of H_2 rate and FE* vs. *current*

Faradaic efficiency

Purity-corrected Faradaic efficiency (FE) remains high and essentially mode-invariant once gas purity is accounted for. As shown in Figure 4a, FE lies between 65.6 and 66.8 % across all currents and both modes. At 1.0 A, FE is 65.9 % (electrolysis) and 66.5 % (sono-electrolysis); at 0.8 A, 66.2 % (electrolysis) and 66.8 % (sono-electrolysis); and at 0.6 A, 65.6 % (electrolysis) and 66.2 % (sono-electrolysis).

The combined presentation in Figure 4c shows that the slightly higher hydrogen output under ultrasound is achieved without any measurable loss in current efficiency: the production rate increases while FE stays essentially constant within experimental variability. From an electrochemical perspective, this does not indicate a competing reaction channel or a measurable change in the overall HER/OER stoichiometry under the present conditions; rather, it is more consistent with changes in transport and bubble dynamics near the electrodes. This pattern matches prior sono-electrochemical observations in which ultrasound improves bubble clearance and surface renewal yet preserves current efficiency when purity corrections are applied [4,21,22].

In the context of alkaline HER research, many studies improve performance by modifying electrocatalyst composition or morphology, such as Ni-MoO_2 cathodes or Ni-Fe phosphide/selenide materials that lower HER overpotential and increase exchange current density through changes in surface chemistry and active sites [23,24]. By contrast, the present H-type cell deliberately keeps the electrochemical interface (materials, geometry, electrolyte) unchanged and uses ultrasound as

a physical process-intensification handle. The nearly unchanged FE therefore supports the interpretation that, in this benchmark configuration, ultrasound primarily alters gas-liquid-solid transport rather than intrinsic HER/OER selectivity.

Specific energy consumption and electrical energy efficiency

Specific energy consumption

On an electrolyzer-electrical basis, the specific energy consumption (SEC) is lower under ultrasound at all three applied currents (Figure 5). Relative to silent electrolysis, the sonicated condition reduces SEC by 20.8 kWh kg^{-1} (≈2.1 %) at 1.0 A, 13.9 kWh kg^{-1} (≈1.7 %) at 0.8 A, and 10.6 kWh kg^{-1} (≈1.6 %) at 0.6 A; the corresponding pairwise values are 973.9 *vs.* 953.1, 807.8 *vs.* 793.9 and 678.5 *vs.* 668.0 kWh kg^{-1} for electrolysis and sono-electrolysis, respectively. These reductions are statistically consistent with the sustained voltage differences discussed in the cell-voltage analysis below and accord with prior observations that ultrasound can reduce the electrical work required to sustain gas evolution by mitigating bubble-induced resistances at the interface and in the near-electrode electrolyte [25,26].

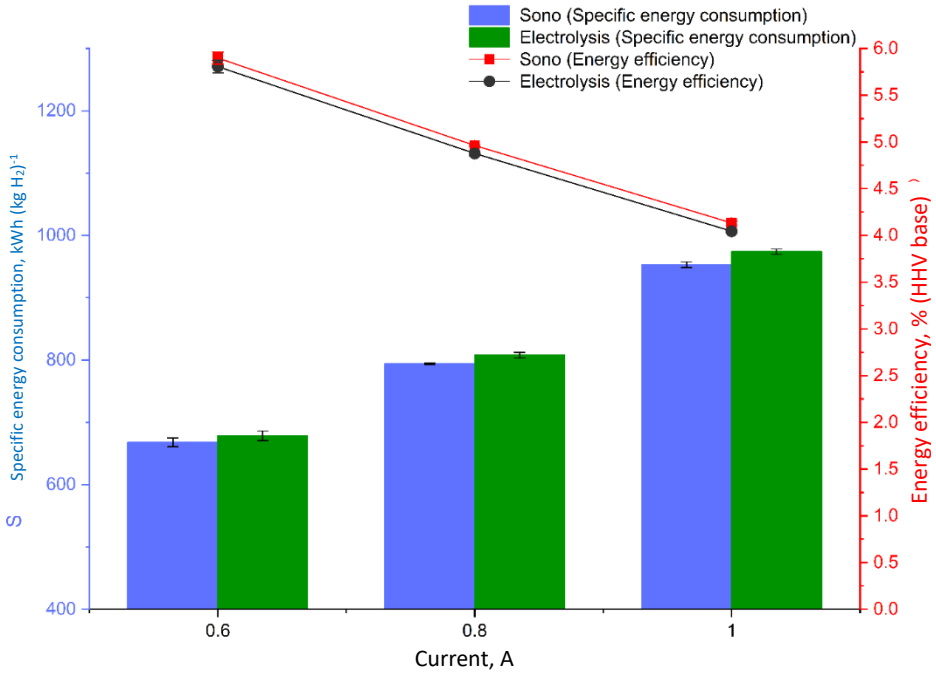

Figure 5. *Specific energy consumption and HHV-based energy efficiency vs. current*

Importantly, the SEC reported here is defined on an electrolyzer-electrical basis and therefore excludes the acoustic power input. In the present study, this boundary is adopted deliberately to isolate the electrical response of the H-type cell to ultrasound-assisted bubble management under otherwise matched galvanostatic and thermal conditions. Accordingly, the reported SEC decrease should be interpreted as a device-internal electrical benefit within the electrolyzer, rather than as a confirmed full-system energy advantage. Recent experiments in alkaline media have directly visualized bubble-layer thinning and cell-voltage reduction under ultrasonication, supporting the link between acoustic agitation, improved gas removal, and reduced electrical work at fixed throughput [22,25,27].

It should be emphasized that, because of the small geometric area, membrane separation, and limited electrolyte volume, the absolute SEC values of the present device are much higher than those of industrial alkaline water electrolysis (AWE) stacks. They should therefore be interpreted as

device-internal benchmarks rather than techno-economic targets. Reviews on separators and membranes for AWE highlight how strongly cell geometry, separator thickness, and ionic path length influence energy consumption [4]. Within this intentionally constrained geometry, however, the relative SEC difference between silent and sonicated operation remains a useful and internally consistent indicator of the extent to which ultrasound can relieve bubble-related and near-electrode transport losses under the present conditions.

Electrical energy efficiency

On the same electrolyzer-electrical basis, the HHV-based electrical energy efficiency (EE, %) is correspondingly higher under ultrasound at each current, reflecting the SEC changes described above (Figure 5). EE rises by 0.089 % at 1.0 A, 0.085 % at 0.8 A and 0.092 % at 0.6 A, with corresponding pairs of 4.045 *vs.* 4.134 %, 4.878 *vs*. 4.963 %, and 5.810 *vs*. 5.902 % for electrolysis and sono-electrolysis, respectively. The absolute efficiency levels fall within the expected envelope for small, membrane-separated H-type cells once referenced to the hydrogen HHV of 39.4 kWh kg^{-1} [25].

From a process perspective, the modest absolute EE values are typical for compact alkaline cells with pronounced ohmic paths, while the mode-to-mode differences track the average-voltage shifts discussed in the cell-voltage analysis below, precisely the pattern expected when bubble-derived ohmic and concentration losses are trimmed while activation contributions remain largely unchanged [26]. As with the SEC comparison above, however, the present EE comparison reflects the electrical response of the H-type cell itself under otherwise matched conditions and should therefore be interpreted as a device-internal metric rather than as a confirmed full-system efficiency gain.

Cell voltage response and bubble-related losses

To connect the observed electrolyzer-electrical changes to an electrical signature, Figure 6a compares average operating voltages at different currents, while Figure 6b resolves their evolution within the steady-state window. In all cases, the voltage required to maintain a given current is lower under sonication. At 1.0 A, the average operating voltage under ultrasound is lower than the electrolysis baseline by 0.29 V (≈1.18 %); the corresponding advantages at 0.8 A and 0.6 A are 0.15 V (≈0.75 %) and 0.09 V (≈0.56 %), respectively, based on the pairs 24.13 *vs.* 23.84 V, 20.10 *vs.* 19.95 V and 16.73 *vs.* 16.64 V. The time-averaged voltage difference ΔV over 30 to 300 s, summarized in Figure 6c, amounts to 0.28, 0.15 and 0.09 V at 1.0, 0.8 and 0.6 A, respectively. The persistence of a positive ΔV across the steady window indicates a sustained device-internal voltage relief rather than a transient fluctuation within the present measurement window.

From a classical electrochemical standpoint, the cell voltage in alkaline water electrolysis can be written as Equation (16):

$$V_{cell} = E_{rev} + \eta_{act} + iR_{ohm} + \eta_{conc} + \eta_{bubble} \quad (16)$$

where E_{rev} is the reversible potential, η_{act} is the sum of activation overpotentials for HER and OER, iR_{ohm} is the ohmic-voltage drop across the electrolyte, membrane and hardware, η_{conc} is the concentration overpotential, and η_{bubble} is the additional contribution associated with gas bubbles partially blocking the electrode surface and current paths [25,28]. In the present setup, the electrode materials, electrolyte composition and geometric configuration are identical between modes, and the exposure time is short. Under these matched conditions, large changes in E_{rev} are not expected, and the present measurements do not independently resolve each contribution in the above expression. The equation is therefore used here as an interpretive framework for discussing the observed mode-to-mode voltage differences rather than as a full mechanistic decomposition.

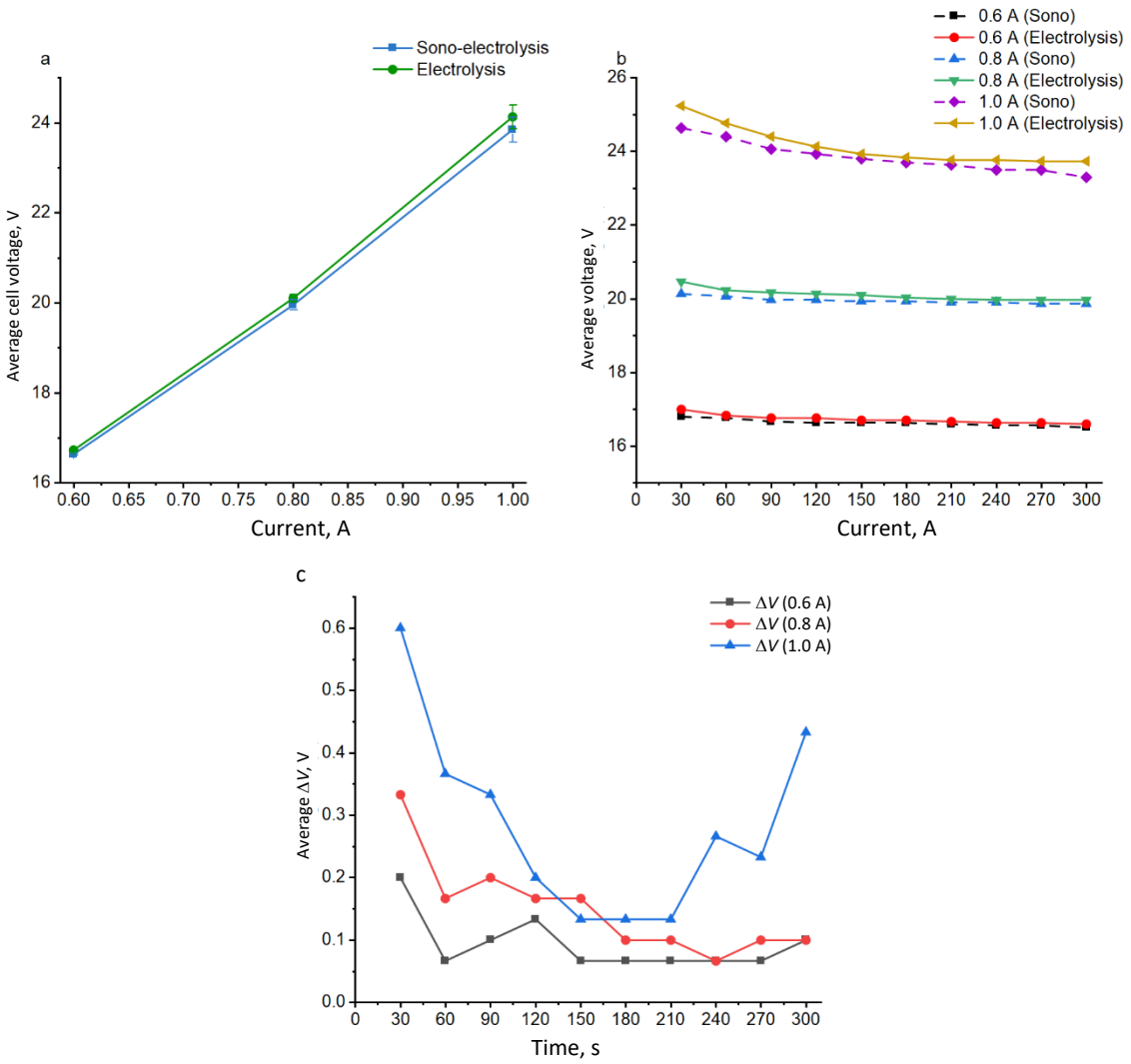

Figure 6. *Operating voltage and time-averaged ΔV: (a) average cell voltage* vs. *current; (b) cell voltage* vs. *time; (c) time vs. averaged ΔV for each current*

Recent analyses of bubble evolution dynamics in alkaline water electrolysis have quantified how increasing gas coverage at the electrode surface increases cell potential and have argued that any strategy capable of inhibiting bubble accumulation will lower the required voltage at fixed current [28]. Experimental and modelling studies show that bubbles can contribute substantially to both ohmic and concentration losses by increasing effective path length, reducing active area and disturbing local concentration fields [28,29]. Within this framework, the lower voltages observed under sono-electrolysis are most consistently interpreted as arising mainly from reduced bubble-related and near-electrode transport losses, associated with enhanced bubble detachment and improved liquid renewal at the electrode surface.

High-speed imaging and indirect acoustic diagnosis in ultrasound-assisted alkaline cells provide direct support for this interpretation: Kwon *et al*. [27] visualized the hydrogen bubble layer on the cathode and showed that ultrasound thins the bubble layer and decreases the power required for hydrogen production, while Kerboua *et al.* [26] correlated changes in cell resistance with cavitation activity and gas holdup in the electrolyte. The present results are consistent with this picture: ultrasound produces a nearly constant downward shift of the cell voltage at each current level without altering the overall shape of the voltage-time curves, suggesting that a major contribution to the observed Δ*V* arises from alleviation of bubble-induced ohmic and concentration losses rather than from a large change in intrinsic reaction kinetics. Within the present benchmark configuration, this

interpretation should therefore be read as the most plausible explanation of the measured voltage response, rather than as a claim of complete mechanistic separation of all overpotential terms.

Effect of ultrasound intensity and operating window at 1.0 A

For benchmark-oriented comparison at 1.0 A within the present H-type cell configuration, Figure 7 compares three modes at 1.0 A: electrolysis, low-intensity ultrasound (low-sono, 70 %) and high-intensity ultrasound (high-sono, 100 %). The purity-corrected hydrogen production rate follows a clear acoustic-intensity ordering: high-sono ⩾ low-sono ⩾ electrolysis, with absolute values of 4.72, 4.64 and 4.59 mL min^{-1}, respectively. FE remains within a tight, high band of 67.74, 66.53 and 65.88 % (Figure 7a). Taken together, these results show that, within the tested range, increasing ultrasound amplitude is associated with a slightly higher hydrogen throughput without any measurable loss of current efficiency.

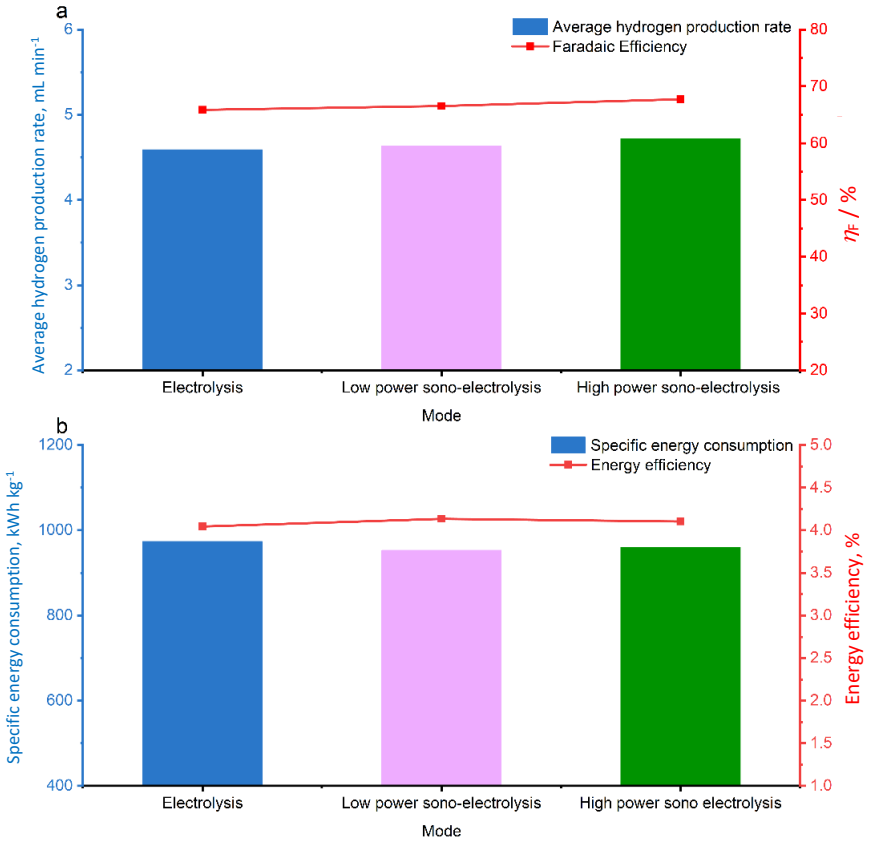

Figure 7. *Mode comparison at 1.0 A: (a) average H_2 production rate and FE for electrolysis, low-sono (70 %), and high-sono (100 %); (b) SEC and HHV-based EE for the same three modes*

The energy metrics present a complementary pattern in Figure 7b. SEC decreases stepwise from 973.9 to 953.01 kWh kg^{-1} and then increases slightly to 960.06 kWh kg^{-1}, while EE increases from 4.05 to 4.13 % and then decreases slightly to 4.10 % across electrolysis, low-sono and high-sono, respectively. Thus, within the present electrolyzer-electrical comparison, low-sono gives the lowest SEC, whereas high-sono gives the highest hydrogen production rate and the largest Δ*V* reduction. Within the tested range, the acoustic field can therefore be treated as a tuneable operating variable in the present benchmark configuration: higher amplitude delivers the largest rate gain, whereas the lowest SEC is achieved at an intermediate intensity. This contrast defines a practical operating window in the present geometry rather than a generalized system-level optimum.

A similar “intermediate-intensity optimum” has been reported for other sono-electrochemical systems. In ultrasound-assisted copper electrodeposition, Mladenović *et al.* [30] showed that

moderate ultrasound intensity provided the most favourable combination of deposit morphology and hardness, whereas higher intensities led to rougher deposits and indications of surface damage, attributed to more violent cavitation and enhanced erosion. In the present alkaline electrolysis system, the onset of graphite anode degradation at high intensity and high current, as discussed in the Limitations and outlook section, points to a similar competition between beneficial bubble-removal and mixing effects and detrimental mechanical and thermal stresses. Sono-electrochemistry and ultrasonic-AWE reviews likewise emphasize that the net effect of ultrasound depends on operating within a window where bubble-management benefits outweigh acoustic dissipation and material wear [4,21,22].

In practical terms, these results indicate that ultrasound amplitude should be regarded as a controllable operating parameter rather than as a universally beneficial intensification lever. Once a baseline level of cavitation sufficient to promote bubble removal is reached, further increases in acoustic intensity may yield only limited additional electrical benefit while increasing mechanical and thermal stress on cell components. Within the present H-type cell geometry and on an electrolyzer-electrical basis, the results therefore support a practical trade-off between hydrogen throughput, SEC, and material durability, and help define the operating window used later in the overall synthesis of this benchmark study.

Synthesis of ultrasound effects

Taken together, the results in the preceding subsections show that ultrasound produces a modest but internally consistent effect in the present membrane-separated alkaline H-type cell. Under fixed current, hydrogen production is slightly higher, purity-corrected Faradaic efficiency remains essentially unchanged once gas purity is accounted for, and the average cell voltage and SEC decrease by approximately 1 to 2 % on an electrolyzer-electrical basis. At the level of the present benchmark, this overall pattern is most consistent with ultrasound acting primarily on bubble-related and near-electrode transport losses, rather than introducing a new reaction pathway or causing a large change in intrinsic reaction kinetics.

In the broader sono-electrolysis literature, substantially larger relative gains in “performance” have sometimes been reported, including double-digit percentage increases in current density, gas production rate, or apparent efficiency, particularly in membraneless or flow-through cells [27]. However, cross-study comparison remains difficult because not all reports simultaneously quantify gas purity, Faradaic efficiency and a clearly defined energy metric, and because cell architectures vary widely, including zero-gap versus millimetre-scale gaps, separator-free versus membrane-separated designs, and different electrode areas and flow conditions. Recent, more detailed studies of ultrasound-assisted alkaline electrolysis have begun to address these issues by combining electrical diagnostics with imaging and more explicit energy accounting, but they also show how strongly the apparent magnitude of the “ultrasound gain” depends on geometry, operating window, and data-treatment choices [31]. This benchmark-oriented interpretation is consistent with the framework proposed in our recent review [20], which argued that ultrasound effects should be assessed against explicit thermal control, gas metrology, and clearly defined SEC boundaries rather than against apparent rate improvements alone.

Within this context, the present H-type cell should be interpreted as a conservative benchmark for what power ultrasound can achieve in a small, membrane-separated alkaline configuration when (i) gas purity and FE are explicitly corrected, and (ii) SEC is reported on a clearly defined electrolyzer-electrical basis. In this geometry, the major irreversible losses arise from finite electrode spacing,

diaphragm resistance and small geometric area, so the scope for ultrasound is correspondingly limited to the fraction of the voltage loss associated mainly with gas coverage and near-electrode transport. Once these bubble-related contributions are partially relieved, the remaining activation and bulk ohmic losses constrain the attainable voltage reduction, even though the trends in Δ*V*, SEC and EE remain internally consistent across modes.

From a process-engineering standpoint, the present data therefore do not position ultrasound as a stand-alone solution to the high energy demand of alkaline water electrolysis. Instead, they support viewing ultrasound as a complementary intensification variable whose effect should be judged against clearly stated thermal and energy-accounting boundaries. Future studies on sono-electrolysis in zero-gap or otherwise advanced alkaline cells can use the present H-type cell as a lower-bound reference: any additional reductions in Δ*V* or SEC beyond the ≈1 to 2 % observed here are more likely to reflect genuine advances in cell architecture, electrode design, coupling strategy, or operating conditions, rather than artefacts arising from uncorrected gas purity, thermal drift, or incompletely defined efficiency metrics.

Limitations and outlook

The present study is intentionally confined to in-cell comparisons in a compact, membrane-separated alkaline H-type cell operated at relatively low total currents (0.6 to 1.0 A) and a single electrolyte composition (2.0 M NaOH). Within this deliberately constrained configuration, the small geometric electrode area, finite electrode gap and diaphragm resistance produce large ohmic contributions and correspondingly elevated absolute SEC and EE values when compared with industrial alkaline water electrolyzers. The quantitative results should therefore be interpreted as device-internal benchmark values rather than techno-economic targets. In other words, the purpose of the present H-type cell is not to demonstrate optimized or competitive system-level performance, but to determine whether any reproducible ultrasound effect remains once geometry, temperature, gas metrology, and performance boundaries are tightly controlled.

A second limitation emerges at the upper end of the tested operating window. At 1.0 A and maximum ultrasonic amplitude, the graphite anode exhibited visible surface degradation and an associated increase in cell resistance, whereas low-intensity ultrasound and silent operation did not show comparable damage. This observation indicates that, in the present H-type cell geometry, acoustic amplitude and current density cannot be increased arbitrarily without compromising electrode integrity. More importantly, it also defines the negative side of the operating window identified in this study: beyond a certain acoustic level, additional cavitation input no longer translates into a proportionate electrical benefit and instead introduces mechanical and possibly thermal penalties. In this sense, the present results support not only the existence of a modest positive window at lower intensity, but also the practical boundary beyond which ultrasound becomes increasingly counterproductive in this configuration.

These constraints also clarify the most relevant directions for future work. On the cell side, reduced electrode gaps, more conductive separators, and mechanically robust electrodes should lower the baseline ohmic penalty and help separate more clearly the relative contributions of activation, ohmic, and bubble-related losses under ultrasound. On the acoustic side, systematic variation of frequency, amplitude and duty cycle, combined with direct diagnostics of bubble dynamics, local temperature, and cavitation activity would help map more rigorously the operating regions in which bubble-management benefits outweigh added acoustic dissipation and materials wear. On the system side, longer-duration testing, durability assessment, and explicit accounting of

acoustic power supply and auxiliary loads will be required to determine whether the modest device-internal gains resolved here can be preserved, amplified, or offset at larger scale.

Taken together, the present findings do not establish ultrasound as a stand-alone solution to the high energy demand of alkaline water electrolysis, nor do they demonstrate a confirmed net energy advantage at the full-system level. Instead, they provide a lower-bound, boundary-aware reference for future studies. If larger reductions in ΔV or SEC are observed in reduced-gap or otherwise advanced alkaline cells under equally explicit thermal and energy-accounting boundaries, such gains will be more credibly attributable to improved cell architecture, electrode design, coupling strategy, and operating conditions rather than to artefacts arising from thermal drift, uncorrected gas purity, or incompletely defined efficiency metrics.

Conclusions

This work investigated the effect of power ultrasound on alkaline water electrolysis in a membrane-separated H-type cell using 2.0 M NaOH and galvanostatic operation at 0.6, 0.8 and 1.0 A. Hydrogen production was quantified by water displacement with gas-purity correction, Faradaic efficiency was evaluated on a hydrogen-fraction basis, and specific energy consumption and HHV-based electrical energy efficiency were determined from the measured voltage-time response. The same electrodes, separator, geometry and current levels were used for silent electrolysis and sono-electrolysis so that any performance differences could be attributed to the presence or absence of ultrasound and, at 1.0 A, to changes in ultrasonic amplitude.

Across all tested currents, ultrasound produced a modest but reproducible device-internal effect under the present conditions. At fixed current, hydrogen production rate increased by approximately 1 %, while the purity-corrected Faradaic efficiency remained essentially unchanged in a narrow band around 66 %, indicating no measurable loss of current efficiency. The time-averaged cell voltage decreased by about 0.09 to 0.29 V between 0.6 and 1.0 A, corresponding to a reduction in SEC of approximately 1.6 to 2.1 % and a corresponding increase in HHV-based electrical efficiency on an electrolyzer-electrical basis. By varying ultrasonic amplitude at 1.0 A, a practical operating window was identified: moderate acoustic intensity minimized electrolyzer-electrical SEC, whereas higher intensity maximized instantaneous hydrogen throughput but accelerated graphite-anode degradation, revealing a trade-off among throughput, electrical response, and material durability.

Taken together, these results are most consistent with ultrasound acting primarily through relief of bubble-related and near-electrode transport losses in the present alkaline H-type cell, rather than through the introduction of a new reaction pathway or a large change in intrinsic reaction kinetics. Within the constraints of the present geometry and operating conditions, ultrasound delivers modest but well-resolved reductions in cell voltage and electrolyzer-electrical SEC while preserving Faradaic efficiency. The resulting dataset should be interpreted as a conservative, device-scale benchmark rather than as evidence of a confirmed full-system energy benefit. Future work should test whether this modest internal signal can be preserved or amplified in reduced-gap cells, with advanced electrodes and improved acoustic coupling, while explicitly including acoustic power, auxiliary loads, and durability in full system-level assessments of green hydrogen production.

Conflict of Interest: *The authors declare no conflict of interest.*

Funding: *This research was funded by the Ministry of Higher Education Malaysia under the Fundamental Research Grant Scheme (FRGS), Project Code: FRGS/1/2023/TK08/USM/02/10.*

References

[1] B. Amini Horri, H. Ozcan, Green hydrogen production by water electrolysis: Current status and challenges, *Current Opinion in Green and Sustainable Chemistry* **47** (2024) 100932. https://doi.org/10.1016/J.COGSC.2024.100932

[2] A. O. M. Maka, M. Mehmood, Green hydrogen energy production: current status and potential, *Clean Energy* **8** (2024) 1-7. https://doi.org/10.1093/CE/ZKAE012

[3] International Energy Agency, Global Hydrogen Review 2024 - Analysis (2024) (accessed September 24, 2025). https://www.iea.org/reports/global-hydrogen-review-2024

[4] D. Henkensmeier, W. C. Cho, P. Jannasch, J. Stojadinovic, Q. Li, D. Aili, J.O. Jensen, Separators and Membranes for Advanced Alkaline Water Electrolysis, *Chemical Reviews* **124** (2024) 6393-6443. https://doi.org/10.1021/ACS.CHEMREV.3C00694

[5] Z. Zhang, C. Gu, K. Wang, H. Yu, J. Qiu, S. Wang, L. Wang, D. Yan, Bubbles Management for Enhanced Catalytic Water Splitting Performance, *Catalysts* **14** (2024) 254. https://doi.org/10.3390/CATAL14040254

[6] S. Yuan, C. Zhao, X. Cai, L. An, S. Shen, X. Yan, J. Zhang, Bubble evolution and transport in PEM water electrolysis: Mechanism, impact, and management, *Progress in Energy and Combustion Science* **96** (2023) 101075. https://doi.org/10.1016/J.PECS.2023.101075

[7] K. Kerboua, O. Hamdaoui, A. Alghyamah, Numerical Characterization of Acoustic Cavitation Bubbles with Respect to the Bubble Size Distribution at Equilibrium, *Processes* **9** (2021) 1546. https://doi.org/10.3390/PR9091546

[8] F. Foroughi, C. Immanuel Bernäcker, L. Röntzsch, B. G. Pollet, Understanding the Effects of Ultrasound (408 kHz) on the Hydrogen Evolution Reaction (HER) and the Oxygen Evolution Reaction (OER) on Raney-Ni in Alkaline Media, *Ultrasonics Sonochemistry* **84** (2022) 105979. https://doi.org/10.1016/J.ULTSONCH.2022.105979

[9] A. Hassani, M. Malhotra, A. V. Karim, S. Krishnan, P. V. Nidheesh, Recent progress on ultrasound-assisted electrochemical processes: A review on mechanism, reactor strategies, and applications for wastewater treatment, *Environmental Research* **205** (2022) 112463. https://doi.org/10.1016/J.ENVRES.2021.112463

[10] P. Adamou, E. Harkou, A. Villa, A. Constantinou, N. Dimitratos, Ultrasonic reactor set-ups and applications: A review, *Ultrasonics Sonochemistry* **107** (2024) 106925. https://doi.org/10.1016/J.ULTSONCH.2024.106925

[11] P. Adamou, E. Harkou, S. Hafeez, G. Manos, A. Villa, S.M. Al-Salem, A. Constantinou, N. Dimitratos, Recent progress on sonochemical production for the synthesis of efficient photocatalysts and the impact of reactor design, *Ultrasonics Sonochemistry* **100** (2023) 106610. https://doi.org/10.1016/J.ULTSONCH.2023.106610

[12] D. Meroni, R. Djellabi, M. Ashokkumar, C. L. Bianchi, D. C. Boffito, Sonoprocessing: From Concepts to Large-Scale Reactors, *Chemical Reviews* **122** (2022) 3219-3258. https://doi.org/10.1021/acs.chemrev.1c00438

[13] M. Sharifishourabi, I. Dincer, A. Mohany, Implementation of experimental techniques in ultrasound-driven hydrogen production: A comprehensive review, *International Journal of Hydrogen Energy* **62** (2024) 1183-1204. https://doi.org/10.1016/j.ijhydene.2024.03.013

[14] C. M. B. De Menezes, D. de M. Sobral, L. B. Dos Santos, M. Benachour, V. A. Dos Santos, Revolutionizing green hydrogen production: the impact of ultrasonic fields, *Brazilian Journal of Environmental Sciences (Revista Brasileira de Ciências Ambientais)* **59** (2024) e1912. https://doi.org/10.5327/Z2176-94781912

[15] H. Su, J. Sun, C. Wang, H. Wang, Study on the influence of ultrasound on the kinetic behaviour of hydrogen bubbles produced by proton exchange membrane electrolysis with water, *Ultrasonics Sonochemistry* **108** (2024) 106968. https://doi.org/10.1016/J.ULTSONCH.2024.106968

[16] S. Merouani, O. Hamdaoui, Y. Rezgui, M. Guemini, Effects of ultrasound frequency and acoustic amplitude on the size of sonochemically active bubbles - Theoretical study, *Ultrasonics Sonochemistry* **20** (2013) 815-819. https://doi.org/10.1016/J.ULTSONCH.2012.10.015
[17] T. Yamamoto, Effect of ultrasonic frequency on mass transfer of acoustic cavitation bubble, *Chemical Engineering Science* **300** (2024) 120654. https://doi.org/10.1016/J.CES.2024.120654
[18] N. H. Merabet, K. Kerboua, Green hydrogen from sono-electrolysis: A coupled numerical and experimental study of the ultrasound assisted membraneless electrolysis of water supplied by PV, *Fuel* **356** (2024) 129625. https://doi.org/10.1016/J.FUEL.2023.129625
[19] N. H. Merabet, K. Kerboua, Dynamic Response of a Sono-Electrolyzer under PV Supply for Hydrogen Production: A Modelling Approach for the Kinetic and Energetic Assessment under Northern Algerian Meteorological Conditions, *Engineering Proceedings* **56** (2023) 117. https://doi.org/10.3390/ASEC2023-15326
[20] C. Zeng, Y. H. Teoh, H. G. How, M. Y. Idroas, T. D. Le, Ultrasound-enhanced water electrolysis for hydrogen production: Mechanisms, metrology and energy metrics, *Journal of Electrochemical Science and Engineering* **16** (2026) 3045. https://doi.org/10.5599/JESE.3045
[21] J. Theerthagiri, J. Madhavan, S. J. Lee, M. Y. Choi, M. Ashokkumar, B. G. Pollet, Sonoelectrochemistry for energy and environmental applications, *Ultrasonics Sonochemistry* **63** (2020) 104960. https://doi.org/10.1016/J.ULTSONCH.2020.104960
[22] F. Foroughi, J. J. Lamb, O. S. Burheim, B. G. Pollet, Sonochemical and Sonoelectrochemical Production of Energy Materials, *Catalysts* **11** (2021) 284. https://doi.org/10.3390/CATAL11020284
[23] G. Tasić, B. Jović, U. Lačnjevac, N. Krstajić, V. Jović, Ni-MoO_2 cathodes for hydrogen evolution in alkaline solutions. Effect of the conditions of their electrodeposition, *Journal of Electrochemical Science and Engineering* **3** (2013) 29-36. https://doi.org/10.5599/JESE.2012.0027
[24] M. Ahmed, A. Hanan, M. N. Lakhan, A. Hussain, I. A. Soomro, B. Niu, Y. Yang, One-pot synthesis of crystalline structure: Nickel-iron phosphide and selenide for hydrogen production in alkaline water splitting: Original scientific paper, *Journal of Electrochemical Science and Engineering* **13** (2023) 575-588. https://doi.org/10.5599/JESE.1721
[25] S. H. Zadeh, Hydrogen Production via Ultrasound-Aided Alkaline Water Electrolysis, *Journal of Automation and Control Engineering* **2** (2014) 103-109. https://doi.org/10.12720/JOACE.2.1.103-109
[26] K. Kerboua, N. H. Merabet, Sono-electrolysis performance based on indirect continuous sonication and membraneless alkaline electrolysis: Experiment, modelling and analysis, *Ultrasonics Sonochemistry* **96** (2023) 106429. https://doi.org/10.1016/J.ULTSONCH.2023.106429
[27] S. Kwon, S. Bae, G. Son, Experimental study of ultrasound-assisted alkaline water electrolysis for hydrogen production, *Journal of Mechanical Science and Technology* **39** (2025) 663-669. https://doi.org/10.1007/s12206-025-0113-9
[28] L. Deng, L. Jin, L. Yang, C. Feng, A. Tao, X. Jia, Z. Geng, C. Zhang, X. Cui, J. Shi, Bubble evolution dynamics in alkaline water electrolysis, *EScience* **5** (2025) 100353. https://doi.org/10.1016/J.ESCI.2024.100353
[29] N. Nagai, M. Takeuchi, M. Nakao, Effects of Generated Bubbles Between Electrodes on Efficiency of Alkaline Water Electrolysis, *JSME International Journal Series B* **46** (2003) 549-556. https://doi.org/10.1299/JSMEB.46.549
[30] I. O. Mladenović, J. S. Lamovec, D. G. V. Radović, V. J. Radojević, N. D. Nikolić, Influence of intensity of ultrasound on morphology and hardness of copper coatings obtained by

electrodeposition: Original scientific paper, *Journal of Electrochemical Science and Engineering* **12** (2022) 603-615. https://doi.org/10.5599/JESE.1290

[31] Y. H. Teoh, S. Y. Liew, H. G. How, H. Yaqoob, M. Y. Idroas, M. A. Jamil, S. U. Mahmud, T. D. Le, H. M. Ali, M. W. Shahzad, Investigating sono-electrolysis for hydrogen generation and energy optimization, *International Communications in Heat and Mass Transfer* **164** (2025) 108980. https://doi.org/10.1016/J.ICHEATMASSTRANSFER.2025.108980